

All optical sensor for automated magnetometry based on coherent population trapping

J.Belfi, G.Bevilacqua, V.Biancalana, Y.Dancheva, L.Moi

CNISM-Unità di Siena, Dipartimento di Fisica - Università di Siena, via Roma 56, 53100 Siena, Italy

An automated magnetometer suitable for long lasting measurement under stable and controllable experimental conditions has been implemented. The device is based on Coherent Population Trapping (CPT) produced by a multi-frequency excitation. CPT resonance is observed when a frequency comb, generated by diode laser current modulation, excites Cs atoms confined in a $\pi/4 \times (2.5)^2 \times 1 \text{ cm}^3$, 2 Torr N_2 buffered cell. A fully optical sensor is connected through an optical fiber to the laser head allowing for truly remote sensing and minimization of the field perturbation. A detailed analysis of the CPT resonance parameters as a function of the optical detuning has been made in order to get high sensitivity measurements. The magnetic field monitoring performances and the best sensitivity obtained in a balanced differential configuration of the sensor are presented.

OCIS 120.4640, 020.1670, 300.6380.

This work has been submitted to JOSA B for publication

[Josa B (7) 2007]

I. INTRODUCTION

Atomic magnetometers, developed since 1960's [1], have today a central role in the field of high sensitive magnetometry with important applications in geophysics, medicine, biology, testing of materials and of fundamental physics symmetries. Technical advances reached in the last years, will make optical magnetometers more suitable than SQUIDs in most of these applications because of the comparable - in some cases, even better [2] - sensitivity and the possibility to operate at room temperature with no need of cryogenic cooling.

Recently a direct measure of geophysical-scale field, with the impressive sensitivity of $60 \text{ fT}/\sqrt{\text{Hz}}$ was demonstrated in a Non-linear Magneto-Optical Rotation experiment [3].

Detection of weak biological-scale magnetic fields (magneto-cardiometry) has been demonstrated using optically pumped magnetometers [4, 5] based on the 'double optical-RF excitation'. Direct RF magnetic excitation, anyway, does not permit the realization of fully optical sensors as RF coils have to be placed next to the vapor cell.

All-optical sensors based on Coherent Population Trapping (CPT) effect can be instead built. CPT effect occurs when two long-lived ground states are coupled to a common excited state by two coherent laser fields. When the frequency difference of the laser fields exactly matches the frequency separation of two not coupled ground levels, the population is trapped in the so called 'dark' state. This is a quantum-mechanical superposition of both ground states that is not coupled to the laser fields. An accumulation of population in such coherent state gives rise to a resonant transparency [6, 7]. CPT resonances have line-widths much narrower than the natural line-width of the corresponding optical transitions. This makes them particularly suitable for precision spectroscopy applications in many other fields besides magnetometry [8, 9] like metrology [10, 11], detection of gravitational waves [12], laser physics [13, 14]

and laser cooling[15].

In this work we present the characteristics of an all-optical magnetometer, working as a compact, automated device able to measure magnetic fields in wide range of amplitudes and time-scales, for example the daily Earth magnetic field variations or weak signals varying in the msec time-scales, superposed on the Earth magnetic field. The sensor works in the magnetically polluted environmental conditions typical of a scientific laboratory. Neither additional RF magnetic field excitation nor particular magnetic field shielding are necessary.

The principle of operation of our CPT magnetometer can be described as follows. Couples of laser fields, such that their frequency separation matches the energy splitting between the Zeeman sub-levels of a given hyperfine ground state of Cs, are produced by frequency modulation of the diode laser junction current in the 10 kHz - 10 MHz range. The obtained frequency modulated radiation is characterized by a very high modulation index ($\sim 10^3$) and the spectral structure of the laser can be seen as a comb of coherent modes with an overall width of the order of the Doppler broadened optical transition. With such a broad band excitation almost all the atomic velocity classes interact with resonant light and furthermore the power absorbed by each single class is very low. The first feature allows us to increase the resonance contrast, the second one reduces the power broadening. It is worth noting that this solution allows us to work without complex laser phase locking systems and, furthermore, without expensive and bulky highly stable microwave oscillators that are, instead, necessary in the case of CPT generation on Zeeman sub-levels of different hyperfine ground states[16].

II. EXPERIMENTAL SETUP AND MEASUREMENT PROCEDURE

A sketch of the experimental setup is presented in Fig.1. The sensor measures the resonant absorption of laser light by Cs vapor contained in a cylindrical cell

2.5 cm in diameter and 1 cm in length. The cell is kept at room temperature and contains 2 Torr of N_2 as a buffer gas. N_2 minimizes the multiple, incoherent re-absorption thanks to the quenching of the resonant fluorescence. The laser radiation is tuned to excite the hyperfine transitions between the ground state with total angular momentum $F_g = 3$ and the excited $^2P_{3/2}$ states with $F_e = 2, 3, 4$.

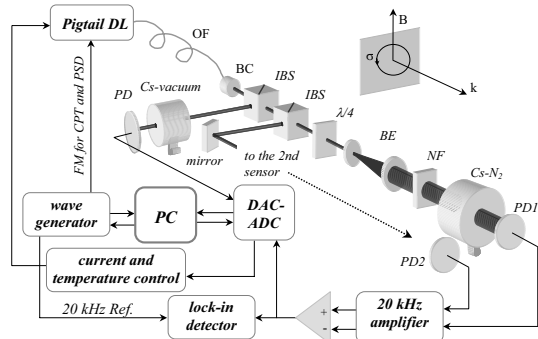


FIG. 1: Experimental setup. OF: optical fiber, BC: beam collimator, IBS: intensity beam splitter, BE: beam expander, NF: neutral filters, PD: photo diode.

The laser is a single-mode edge-emitting pigtail laser ($\lambda = 852$ nm) with 100 mW of laser power and an intrinsic line-width of less than 5 MHz. Optical feedback is avoided by means of 40 dB optical isolator and the laser light is coupled into a 10 m long single-mode polarization-maintaining fiber. The laser head containing the laser chip, the optical isolator and the fiber collimator is closed in a butterfly housing of only 40 cm³. The beam coming from the fiber is collimated and its polarization is transformed from linear to circular using a quarter-wave plate. In order to increase the light-atom interaction time the beam waist is expanded to 4.3 mm and the laser intensity used for atom excitation is reduced to 36 $\mu\text{W}/\text{cm}^2$ using a set of neutral filters. The transmitted laser light is detected and analyzed.

CPT resonance is created when two different Zeeman sublevels are coherently coupled to a third common Zeeman sublevel. The three-level system involved is called Λ system in the case the third common coupled level is the highest in energy, V system in the case it is lowest. In our case a number of Λ and V systems are created with circularly polarized light preserving the selection rules $\Delta m_f = 0, +1$ and $\Delta m_f = 0, -1$. Chains of Λ systems are formed on the $F_g = 3 \rightarrow F_e = 2, 3$ group of transitions, while chains of V systems are formed on the $F_g = 3 \rightarrow F_e = 4$.

The magnetic field under measurement breaks the Zeeman degeneracy and makes adjacent ($|\Delta m_F| = 1$) sublevels separated by $\hbar\mu_0 g_F B = \hbar\omega_L$, where \hbar is the Planck constant, μ_0 is the Bohr magneton, g_F is the Landé factor of the considered ground-state, ω_L is the Larmor frequency and B is the magnetic field strength. In Fig.2, as example, is represented the schematics of Λ -system

chains formation for the $F_g = 3 \rightarrow F_e = 2$ system of transitions.

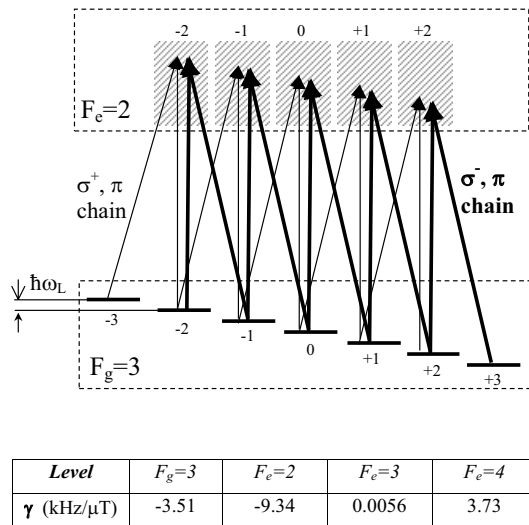


FIG. 2: Representation of Λ -system chains for the $F_g = 3 \rightarrow F_e = 2$ system. The quantization axis is parallel to the magnetic field and perpendicular to the laser beam. Circular polarization is decomposed in two in-quadrature linearly polarized waves, one of which is in turn decomposed in two counter rotating fields circularly polarized around the quantization axis. The complete scheme would involve also the hyperfine components $F_g = 3 \rightarrow F_e = 3, 4$. In the table are reported the gyromagnetic factors γ for all the hyperfine levels of interest.

The RF signal used to produce couples of suitably separated frequency components in the spectral profile of the laser emission is swept in a small interval around the resonant value ω_L . A set of data acquired along the frequency sweep allows for visualizing the CPT resonance profile.

As the magnetic field strengths of interest range from few μT to few mT, the modulation frequency Ω_{RF} ranges from few tens of kHz to few MHz. The Ω_{RF} is generated by a waveform generator (Agilent 33250A 80-MHz Function Generator) that is coupled to the laser by means of a passive circuit specially designed to make the response of the laser rather flat in the frequency range of interest. The circuit uses capacitors to ac couple the RF to the laser junction, and resistors of rather large value (several hundreds Ohm) to convert the voltage to current at the output of the generator. A pair of inductive elements, oriented so that possible spurious magnetic pick-up is canceled, are connected in series with the dc supply in order to prevent the modulating signal from being significantly counteracted by the laser current driver. As an overall, this coupling allows for achieving very large modulation indexes. The envelope of the unresolved frequency components of the resulting comb of laser frequencies can be observed using a Fabry-Perot spectrometer (see Fig.3).

In order to increase the S/N of the detected transmitted light, a Phase Sensitive Detection (PSD) is per-

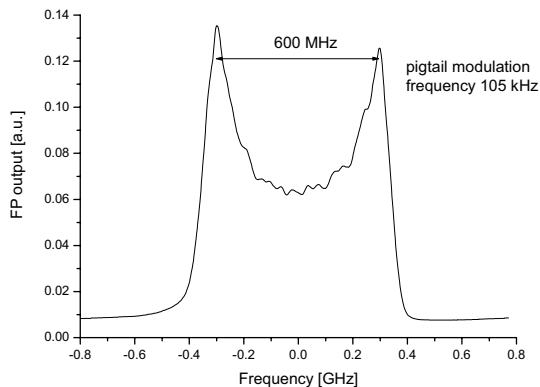


FIG. 3: Pigtail laser spectrum recorded using a confocal Fabry-Perot interferometer with FSR = 1.5 GHz. The modulation frequency is 105 kHz. The inferred modulation index is ~ 2800 .

formed. The Ω_{RF} is thus frequency-modulated at Ω_{PSD} and the atomic response in phase with a reference signal at Ω_{PSD} is extracted. Laser electric field can be expressed by:

$$\vec{E} = E_0 (\hat{x} + i\hat{y}) \exp\{i[\omega_0 t + \varphi(t) + M_{RF} \cos(\Omega_{RF} t + M_{PSD} \cos(\Omega_{PSD} t))]\} + c.c. \quad (1)$$

where \hat{x} and \hat{y} are the usual unitary vectors perpendicular to the laser wave-vector, ω_0 is the optical frequency, $\varphi(t)$ accounts for the laser linewidth invoking for instance the celebrated phase-diffusion model, M_{RF} is the modulation index of the RF modulation and Ω_{PSD} is the PSD modulation frequency with its modulation index M_{PSD} . One typical FM spectrum of the CPT profile is presented in Fig.4 where $\Omega_{PSD} = 20$ kHz and $M_{PSD} = 1$. The central feature is used for magnetic field determination.

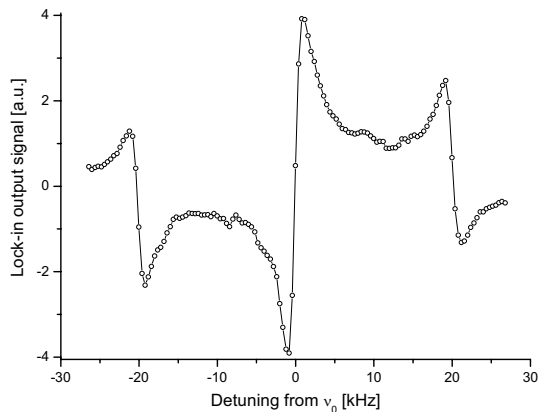


FIG. 4: FM spectroscopy of the CPT resonance at modulation frequency of 20 kHz with deviation of 20 kHz. .

An improvement in the noise rejection and hence in the sensitivity can be achieved using a differential sensor. Such arrangement is very appropriate when a registration of very weak magnetic fields is desired [16]. In this

case, two identical sensors are assembled in parallel, at a distance of 11 cm. The light is coupled to the second arm of the sensor using an intensity beam splitter (see Fig.1). When evaluating the efficiency of the differential setup in rejecting the noise, we distinguish three kinds of noise contribution. The first is due to the detection and amplification stages. This contribution, which is generally smaller than the others is increased (nominally by a factor $\sqrt{2}$). The second kind is due to intensity fluctuations of the laser emission (rather small in our case) and to frequency noise of its optical frequency, in turn discriminated by the Doppler profile. This kind of noise is effectively rejected. As a third kind one can consider the noise due to magnetic field fluctuations generated by magnetic sources different from the one under examination (e.g. consider the case of Earth magnetic field fluctuation while measuring weak biological fields generated by close sources). In this case, provided that both the Cs cells are in conditions of CPT resonance, the differential sensor responds to the (usually very small) gradients of the field generated by far-located sources (while their common mode field is canceled) and to the field generated by sources (if any) located very close to one of the two cells. In this sense depending on the application, the differential setup can be used either as a gradiometer or as detector of field variations produced by close sources placed in magnetically polluted environment.

The components of both arms of the differential sensor, *i.e.* the fiber collimator, quarter-wave plates, beam expanders, neutral filters, Cs-N₂ cells and the PDs (we use large area, low noise, non-magnetic photo diodes) including a reference Cs-vacuum cell are assembled in a separate plate and can be placed away from the instrumentation. All used materials are highly non-magnetic so that the sensor does not perturb the magnetic field to be measured. In the condition of our Laboratory an improvement of the signal to noise ratio (S/N) of a factor of 5 was obtained.

A. CPT profile and noise

The magnetic field measurement operatively consists in the determination of the central frequency ν_0 of the resonance profile ($2\pi\nu_0$ is the estimate of ω_L). The registered CPT profile, read at the output of the lock-in, reproduces the first derivative of the CPT (reduced absorption) resonance. One typical CPT profile is presented in Fig.5. The error bars are evaluated by the lock-in amplifier from the standard deviation of the output signal in steady conditions. Routinely, the noise measurement is done only once - after setting the lock-in operation parameters, because it is a time consuming operation, and can not be performed at each step.

The central frequency and the linewidth of the resonance are estimated by means of a best fit procedure. The fitting function is the first derivative of a Lorentzian profile with central frequency ν_0 and FWHM Γ . It allows

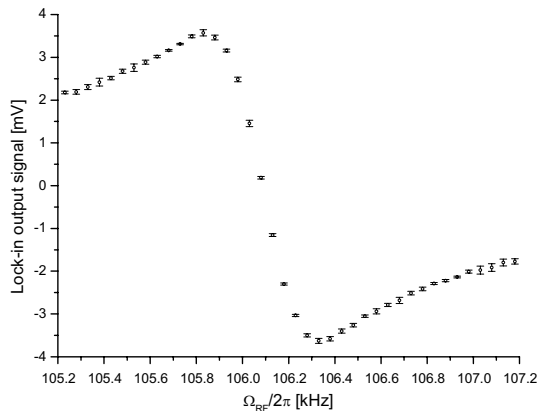


FIG. 5: Typical CPT profile observed when scanning the modulation frequency around $\omega_L/2\pi$. The lock-in time constant is 30 ms with 12 dB/oct output filter which determines the detection bandwidth of 4.16 Hz. The linewidth resulting from the fit procedure is $\Gamma = 700$ Hz.

for achieving an excellent agreement of fit with the data detected in the experimental conditions described above, provided that the RF scan is performed in a narrow range around the ν_0 . Discrepancies appear for wider ranges of scan. In this condition we found that adding a secondary small, odd function with the same center as the principal derived Lorentzian, removes the discrepancy in the wings, making the fit result insensitive to the position of the center of the resonance with respect to the center of the scan. We used another (smaller and broader) Lorentzian derivative, to take into account such slower decays in the wings.

The uncertainty on the resonant frequency evaluated by the fit procedure, converted in magnetic field units, is consistent with the following estimation:

$$\frac{\Delta B}{\sqrt{\Delta\nu}} = \frac{1}{\gamma} \times \frac{n\sqrt{\tau}}{\partial V/\partial\nu}, \quad (2)$$

where n is the noise level at the output of the lock-in, τ is the measuring time (it depends on both the time-constant and the slope of the output filter in the lock-in), $\partial V/\partial\nu$ is the slope of the CPT curve and γ is the atomic gyromagnetic factor.

The noise level n can be estimated, as written above, by direct measurement from the lock-in amplifier, while the resonance central slope is simply related to the ratio between the amplitude and the FWHM of the signal. In typical working conditions, n amounts to about 3 times the photo-current shot-noise level, and is mainly due to fast laser frequency fluctuations (the measured noise decreases to the expected shot-noise level provided that the optical frequency is tuned out of resonance), while the FWHM line-width is about 700 Hz. The CPT parameters, $1/\gamma$ factor in our configuration and the noise pattern of our registration system, including the magnetic noise in the Laboratory, set the ultimate sensitivity of the sensor to 260 pT/ $\sqrt{\text{Hz}}$ according to Eq. 2. This sensitivity

limit is far above the very ultimate theoretical limit of the sensitivity, which considering only contribution of the light-atom interaction volume and Cs-Cs spin exchange collisional rate is 8 fT/ $\sqrt{\text{Hz}}$ [17].

In general, in order to improve the sensitivity limit versus the theoretical one, one has to reduce the resonance line-width Γ , to increase the signal-to-noise ratio and to work in a highly shielded room.

The main CPT resonance broadening mechanism, in our case, is the limited light-atom interaction time and contributes to the total linewidth by an amount of the order of 600 Hz. Unshielded environmental conditions and, in particular, magnetic field gradients and AC magnetic fields, also contribute to the CPT line broadening. The maximum magnetic field gradient is estimated to be in the range of 80 nT/cm, leading to, worst case, a broadening contribution of the order of 280 Hz. AC magnetic fields contribute, instead, mainly with the 50 Hz and its harmonics spectral components, with an overall intensity of 40 nT, determining a corresponding broadening of about 140 Hz. Smaller broadening contributions are furthermore given by the light shift and the non-linear Zeeman effect [18].

III. PC AUTOMATED CONTROLS

The experimental procedure is totally controlled by a dedicated LabView program. The program is used to synchronously communicate with the lock-in amplifier and the RF wave generator so that the CPT response can be recorded in appropriate and reproducible conditions.

A. Automated registration of the CPT profile and subsequent fit

The CPT profile is registered by querying the lock-in output after having set the RF and having waited the settling time. Alternatively, as described below, the program performs numerically PSD, using large data sets produced by a 16 bit ADC card. The program also contains routines devoted to an on-line analysis of the collected data. In particular, after that each RF scan is completed, a minimum χ^2 fit procedure is launched to determine the parameters of CPT resonance profile.

When performing numerical PSD, in contrast with what reported in Section II A, the noise level is evaluated at each Ω_{RF} step. In both cases, we obtain rather good values for the minimized χ^2/DoF (degrees of freedom), demonstrating the reliability of the noise estimation and the suitability of the fitting procedure.

B. Numerical PSD

The external lock-in amplifier (bulky and expensive) can be replaced by a compact ADC card. We successfully tested and used a system based on a commercial 16 bit, 50 kS/s card USB interfaced to the PC and sets to operate at 40 kS/s. The principle of operation was slightly changed with respect to the one of the lock-in amplifier. Specifically, the RF is externally frequency modulated at 20 kHz using a square wave signal obtained by scaling by two the frequency of a clock signal generated by the ADC card. Consequently, the ADC data array y corresponds to high and low values of the RF, accumulated in the even (y_{2i}) and odd (y_{2i+1}) elements, respectively. The PSD signal and its uncertainty are then obtained by considering the N -size array of differences $\delta_i = y_{2i+1} - y_{2i}$ and evaluating the average $\langle \delta \rangle = \sum_i \delta_i / N$ and the standard deviation $[\sum_i (\delta_i - \langle \delta \rangle)^2 / N]^{1/2}$ scaled by \sqrt{N} , respectively.

The number $2N$ of the acquired data is chosen accordingly to the desired integration time of the PSD system, and its upper limit is set by the size of the data buffer in the ADC card (64 kB / 2 Bytes = 32767 readings which corresponds to 0.8 sec integration time). It is worth noting that the relatively large amount of data to be transferred makes the choice of USB 1.0 devices not very advantageous, because it introduces a relevant dead-time at each measurement.

C. Frequency stabilization on the Doppler profile

Multi-frequency diode laser comb excitation is suitable for producing narrow and high contrast CPT signals in free-running lasing conditions. The optical frequency stabilization by the laser current and temperature controllers provides the needed short-term stability. Such passive stabilization method works well over time intervals of the order of 1 min, but over longer time-scales slow drifts of both temperature and current make it unsuitable. For this reason a long-term active stabilization system must be employed, allowing for relatively rough (accurate within some MHz) but reliable re-adjustments of the optical frequency.

We adopted a simple method based on a commercial USB ADC-DAC card with 12 bit resolution, which periodically and automatically (e.g. once per minute) performs a scan all over the Doppler profile, numerically determines center and width of the absorption curve, and finally provides a dc signal, which, sent to the modulation input of the laser current driver, establishes detuning with respect to the maximum of the absorption profile, in terms of the measured linewidth. In spite of the low cost and simplicity, such sub-system was demonstrated to be very effective and reliable for long-term compensation of the optical frequency drifts. Furthermore it made the whole system comfortable to be operated during the op-

timization as well as suitable for applicative long-lasting use.

Additionally, we note that such approach, at the expense of periodically suspending the CPT measurement for a few seconds, does not need any additional laser modulation (which would have effect on the CPT measurement) or external modulation elements (such as Electro optical modulators), which would make the set-up much more complex and expensive.

We have quantified the root mean square fluctuations $\Delta\nu_{opt}^{rms}$ of the optical frequency, i.e. the center of the broadband laser spectrum used for CPT creation, observing the apparent fluctuation of the fitted Doppler maximum position when scanning the laser current in the same range of nominal values over the Doppler absorption. From the observed rms variation of the fitted maximum we get $\Delta\nu_{opt}^{rms} \simeq 2\text{MHz}$ over time scales of the order of 1 sec.

D. Servo locking at the center of the CPT resonance

When a higher rate in the magnetic field measurements is required the time needed to perform RF scan in order to determine the center of the CPT resonance can be avoided performing single readings of the lock-in output. This fast operation uses the central, essentially linear, slope of the CPT resonance (the Lorentzian derivative profile) resulting from the fit, to convert the lock-in output voltage in frequency units and hence in field units.

Initially, one complete Ω_{RF} scan is accomplished, the fitting procedure runs, and, provided that the χ^2 / DoF is reasonably close to unity, the best-fit parameters are passed to the routine devoted to evaluate the field from single readings of the lock-in and to keep Ω_{RF} locked to the resonance center.

The fit procedure gives the values of both the slope $\frac{dV}{d\nu}$ and the offset V_0 at the center of resonance ν_0 . When the single reading procedure starts working, Ω_{RF} is set at ν_0 , and the lock-in output V is queried. The deviation $\Delta V = V - V_0$ is used in a linear approximation to obtain a new estimate of the central frequency $\nu_0 + \Delta V / (dV/d\nu)$ and hence of the field. At each step, Ω_{RF} is updated to the new estimated ν_0 in order to keep the system working at the center of the CPT resonance, with the double aim of maintaining the linear estimation appropriate, and preventing possible large drifts of the field from bringing the system out of the CPT resonance.

The lock-in time-constant can be selected with different values for the scan and the single-reading operations. Obviously, to obtain a comparable noise rejection in single-reading operation it is necessary to increase the time-constant. The lock-in settling time derived from the time-constant and the lock-in output filter slope is taken into account in the lock operation in order to update Ω_{RF} with a rate R allowing for locking the system at the actual center of resonance with the maximum speed, but

without risks of oscillations.

Ω_{RF} is actually updated at the rate R' of the readings (this value is limited by the RS232 communications, and generally exceeds R) consequently, the Ω_{RF} increment is scaled by a factor R/R' .

The evaluated magnetic field is immediately saved on disk, possibly simultaneously with other reference signals (for instance, in the perspective of applications in magneto-cardiography, ECG signals will be saved as a reference, in view of offline analysis to be performed over long-lasting acquisitions).

IV. SIGNAL OPTIMIZATION, PERFORMANCES AND LIMITS

The dependence of the amplitude of the CPT resonance as a function of the laser optical detuning is shown in Fig.6a, where the CPT amplitude, the Doppler broadened fluorescence line and the frequency position of the hyperfine transitions are reported. The CPT resonance amplitude shows a two-lobe structure that reflects the bridge-shaped spectral intensity profile shown in Fig.3, with the two maxima separated nearly by the same amount (about 600 MHz). The reason for the vanishing resonance at intermediate detunings lies in the opposite phase of the beating at Ω_{RF} of the FM laser spectrum. Actually, each couple of adjacent sidebands in the laser spectrum, with their amplitudes J_m, J_{m+1} , which produce a beating signal at Ω_{RF} , contains one odd and one even Bessel function so that, due to the fact that $J_{-m}(M) = (-1)^m J_m(M)$ the beat phases is opposite for the couple $(m, m+1)$ and $(-m, -(m+1))$ respectively, i.e. for the couples belonging to the right and left wings of the bridge. From this point of view, depending on the optical detuning, a synchronous excitation [3, 19] of different velocity classes of atoms is performed, having a unique phase in the case where one side only of the bridge is in resonance with the Doppler profile, and two opposite phases when the bridge center coincides (about) with the Doppler center. A deeper analysis puts in evidence that the two lobes in Fig.6a are different in amplitude, with higher values on the blue side. This is related to the dominance of the $F_g = 3 \rightarrow F_e = 3$ and $F_g = 3 \rightarrow F_e = 4$ transitions on the blue wing of the Doppler line. On the other hand, the CPT resonance vanishes when the laser is tuned in the vicinity of the $F_g = 3 \rightarrow F_e = 2$ transition, and the maxima of the two lobes are symmetric with respect to such detuning, accordingly with the fact that this latter, closed transition gives the most relevant contribution to the CPT.

Besides the evident variation of the resonance amplitude discussed above, changing the optical detuning determines also a variation both in the resonance linewidth (Fig. 6 b) and in the resonance center frequency. The linewidth dependence on optical frequency affects mainly the sensitivity of the instrument according with Eq. 2. The shift of the CPT resonance center versus optical de-

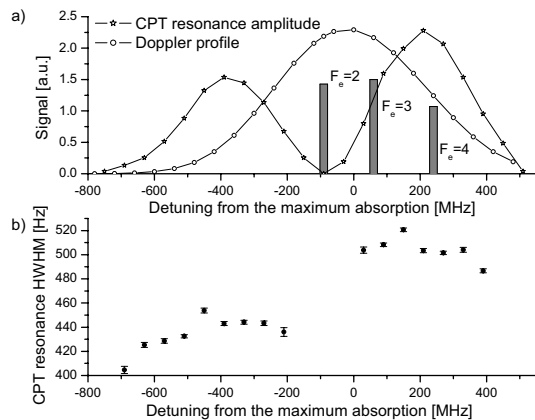


FIG. 6: a) CPT resonance amplitude versus optical detuning (zero frequency corresponds to the maximum of the Doppler profile). The frequency position of the three hyperfine transitions are marked with respect to the calculated Doppler profile. b) CPT HWHM versus optical detuning.

tuning, also called light-shift or ac Stark effect, is due to the finite dephasing rate among ground states involved in the CPT preparation (see [[20, 21]]). This effect represents an essential systematic error in the determination of the CPT resonance center and then affects both the accuracy and the sensitivity of the magnetometer. The CPT center frequency shift rate versus optical detuning is presented in Fig.7 for laser intensity of $36 \mu\text{W}/\text{cm}^2$.

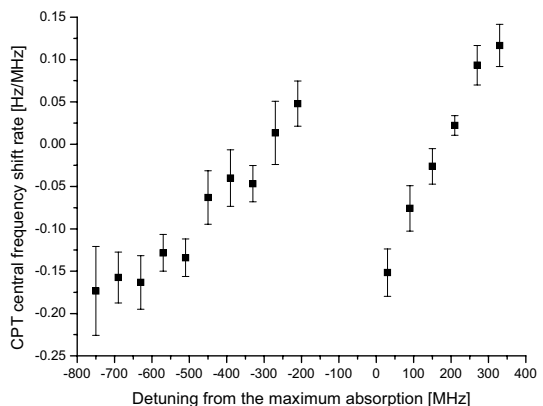


FIG. 7: CPT resonance center shift rate depending on optical detuning for laser intensity of $36 \mu\text{W}/\text{cm}^2$. The value given at each point is obtained by averaging the difference in the CPT resonance centers measured 30 MHz above and 30 MHz below the corresponding value of the detuning from the maximum absorption. Error bars represent the standard deviation of each data set consisting of about 150 measurements.

The optimal optical detuning, in view of best magnetometer operation, is around 400 MHz red detuning, where the light-shift rate passes through a minimum value and the CPT resonance has lower linewidth.

A. Magnetic field monitoring

The magnetometer performance was checked by registration of the Earth magnetic field variation in time. A record of few hours continuous magnetic field registration with our magnetometer [22] is shown in Fig.8 together with the corresponding data of the L'Aquila geomagnetic station [23].

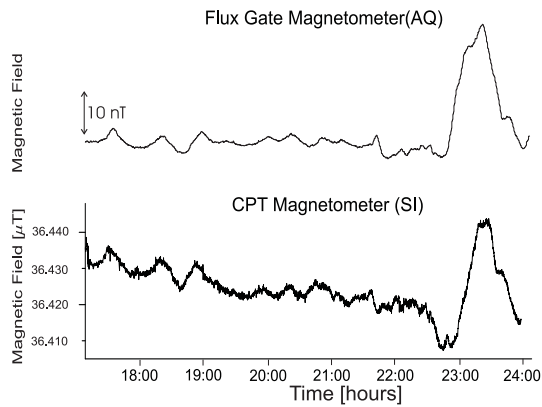


FIG. 8: Long lasting monitor of the Earth magnetic field, comparison between two different independent measurements. Upper trace: acquisition of the fluctuations of the Earth magnetic field modulus measured by the 3-axes flux-gate magnetometer in the Geophysical Institute of L'Aquila. Sampling rate is one point per minute. Lower trace: acquisition of the modulus of the Earth magnetic field in the Physics Department of the University of Siena. In this case the sampling rate is about 1 point each 8 sec. Both the direction and the strength of the magnetic field are strongly influenced by the presence of ferromagnetic objects in the laboratory and in the structure of the building.

Both the procedures, when fitting the CPT resonance for determination of its center and using fast acquisition, were considered and investigated. In the first one, the whole CPT profile is registered and fitted as described above. In this case the measuring time, limited by the time necessary for CPT profile registration together with the subsequent data analysis, is of the order of 8 sec. Such procedure does not make possible to register fast magnetic field variations and in this respect can find application in geophysics, archaeology, material science, etc.

A trace of the Earth magnetic field variation obtained in fast operation is shown in Fig.9. In this case the acquisition rate was increased by a factor of 40 (210 ms per reading).

The magnetometer sensitivity to weak magnetic field variations superimposed on the Earth magnetic field was determined when working in the differential configuration. For this purpose, a calibrated variable magnetic field was applied using multi-turns coil, placed half a meter away from the sensor. The calibration of the magnetic field strengths on the two arms of the sensor produced by the coil was done using the magnetometer itself. The magnetometer response to a slow and weak variation of

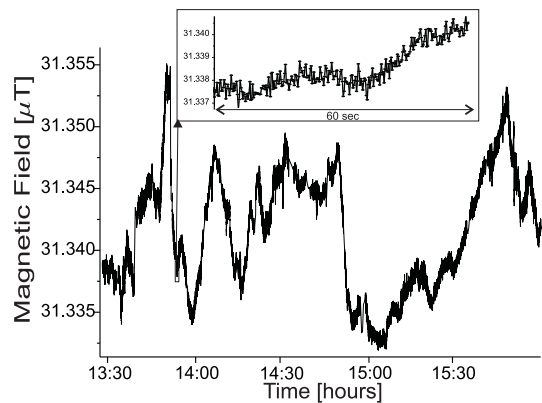


FIG. 9: Magnetic field variation registration in single reading operation. In the inset is sketched the zoom over 1 min acquisition.

the magnetic field in time is presented in Fig.10. It can be seen that variations in the magnetic field difference of the order of 300 pT_{p-p} are well resolved. The inferred magnetometer sensitivity in differential configuration is $45 \text{ pT}/\sqrt{\text{Hz}}$.

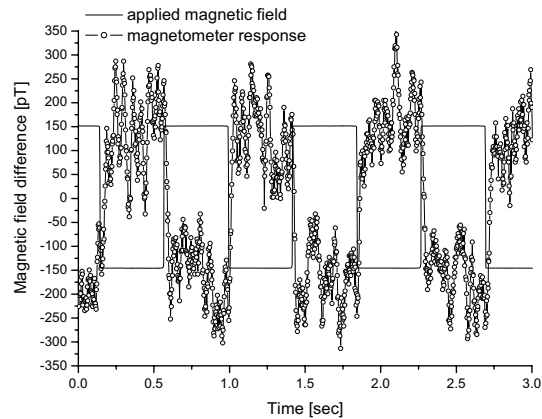


FIG. 10: The magnetometer response to a 300 pT_{p-p} , 0.8 Hz square-wave magnetic signal registered in differential configuration with a band-width determined by the lock-in time constant of 3 msec, 12 dB/oct output filter and 10 averages.

V. CONCLUSIONS

We have built an all-optical magnetometric sensor supplied with a PC-automated control of the experimental parameters and an absolute magnetic field measurement data acquisition system.

CPT resonance creation by a kHz-range frequency-modulation of a free running diode laser in totally unshielded environmental conditions is demonstrated and an accurate characterization of the optimal experimental parameters relative to the generation of broad band frequency comb spectrum and to the detection strategy is

also given. We presented, furthermore, a detailed analysis of the dependence of CPT resonance amplitude and width on the optical frequency tuning, thus determining the optimal detuning from the central frequency of the single-photon absorption spectral profile. The magnetometer performs long term continuous monitoring of magnetic field in the Earth-field range providing a very sensitive tool for small magnetic field variation registration. We plan to routinely and systematically publish such data almost in real-time (preliminary sets are available in Ref.[[22]]), with the aim of making our system useful for remote Earth magnetic field continuous observations and possible comparisons with measurements

performed elsewhere.

The best sensitivity, inside a totally unshielded environment, reached in the differential balanced configuration is $45 \text{ pT}/\sqrt{\text{Hz}}$.

Acknowledgments

We thank S. Cartaleva and A. Vicino for useful discussions and A. Barbini for the technical support. This work was supported by the Monte dei Paschi di Siena Foundation.

-
- [1] A. L. Bloom, "Principles of operation of the rubidium vapor magnetometer", *Appl. Opt.* **1**, 61-68 (1962).
- [2] I. K. Komins, T. W. Kornack, J. C. Allred, M. V. Romalis, "A subfemtotesla multichannel atomic magnetometer", *Nature* **422**, 569-599 (2003).
- [3] V. Acosta, M. P. Ledbetter, S. M. Rochester, D. Budker, D. F. Kimball, D. C. Hovde, W. Gawlik, S. Pustelny, J. Zachorowski, "Nonlinear magneto-optical rotation with frequency-modulated light in the geophysical field range", *PRA* **73**, 053404 (2006).
- [4] G. Bison, R. Wynands, and A. Weis, "A laser-pumped magnetometer for the mapping of human cardiomagnetic fields", *Appl.Phys. B* **76** (3), 325-328 (2003).
- [5] G. Bison, R. Wynands, and A. Weis, "Dynamical mapping of the human cardiomagnetic field with a room-temperature, laser-optical sensor", *opt. expr.* **11**, 904-909 (2003).
- [6] G. Alzetta, A. Gozzini, L. Moi, and G. Orriols, "An experimental method for the observation of r.f. transitions and laser beat resonances in oriented Na vapors", *Nuovo Cimento* **B 36**, 5-20 (1976).
- [7] E. Arimondo and G. Orriols, "Nonabsorbing atomic coherences by coherent two-photon transitions in a three-level optically pumping", *Lett. Nuovo Cimento* **17**, 333-338 (1976).
- [8] M. Scully and M. Fleischhauer, "High-sensitivity magnetometer based on index-enhanced media", *PRL* **69**, 1360-1363 (1992).
- [9] M. Fleischhauer and M. Scully, "Quantum sensitivity limits of an optical magnetometer based on atomic phase coherence", *PRA* **49**, 1973-1986 (1994).
- [10] J. E. Thomas, P. R. Hemmer, S. Ezekiel, C. C. Leiby Jr., R. H. Picard, C. R. Willis, "Observation of Ramsey Fringes Using a Stimulated, Resonance Raman Transition in a Sodium Atomic Beam", *PRL* **48**, 867-870 (1982).
- [11] P. Hemmer, M. Shahrair, H. Lamela-Rivera, S. Smith, B. Bernacki and S. Ezekiel, "Semiconductor laser excitation of Ramsey fringes by using a Raman transition in a cesium atomic beam", *JOSA B* **10**, 1326-1329 (1993).
- [12] C. Caves, "Quantum-mechanical noise in an interferometer", *PRD* **23**, 1693-1708 (1981).
- [13] S. Harris, "Lasers without inversion: Interference of lifetime-broadened resonances", *PRL* **62**, 1033-1036 (1989).
- [14] O. Kocharovskaya, "Amplification and lasing without inversion", *Phys. Rep.* **219**, 175-190 (1992).
- [15] C. Cohen-Tannoudji and W. Phillips, "New mechanism for Laser cooling", *Physics Today* **43**, 33-40 (1990).
- [16] C. Affolderbach, M. Stähler, S. Knappe, R. Wynands, "An all-optical, high-sensitivity magnetic gradiometer", *Appl.Phys. B* **75**, 605-612 (2002).
- [17] J.C. Allred, R.N. Lyman, T.W. Kornack and M.V. Romalis, "High-Sensitivity Atomic Magnetometer Unaffected by Spin-Exchange Relaxation", *PRL* **89**, 130801 (2002).
- [18] Ch. Andreeva, G. Bevilacqua, V. Biancalana, S. Cartaleva, Y. Dancheva, T. Karaulanov, C. Marinelli, E. Mariotti, L. Moi, "Two-color coherent population trapping in a single Cs hyperfine transition, with application in magnetometry", *Appl.Phys. B* **76**, 667-675 (2003).
- [19] D. Budker, W. Gawlik, D. F. Kimball, M. Rochester, V. V. Yashchuk, A. Weis, "Resonant nonlinear magneto-optical effects in atoms", *Rev.Mod.Phys.* **74**, 1154-1201 (2002).
- [20] E. Arimondo, "Coherent population trapping in laser spectroscopy", *Prog. Opt.* **35**, 257-354 (1996).
- [21] C. Cohen-Tannoudji, J. Dupon-Roc, G. Grynberg, *Atom-Photon Interaction*, (Wiley, New York, 1992).
- [22] <http://magnetometer.fisica.unisi.it/lab>
- [23] <http://www.ingv.it/geomag/laquila.htm>